



## 41 1 Introduction

42

43 The ability to make comparisons between sensory stimuli of different intensities has profound  
44 survival value for most organisms. Animals might benefit from choosing the ripest fruit based  
45 on colour, swimming towards the warmest patch of ocean, or selecting the mate with the  
46 loudest roar. Understanding the features of the central nervous system that limit such  
47 sensory discriminations has been a focus of research in many areas of psychology and  
48 neuroscience, from early work in humans (c.f. Weber's law, Fechner, 1912), and experiments  
49 with model organisms (Busse et al., 2011; Hecht & Wald, 1934) to studies using contemporary  
50 neuroimaging techniques (Boynton, Demb, Glover, & Heeger, 1999).

51

52 A widely studied perceptual task is the ability to discriminate between visual stimuli of  
53 different contrasts. Human contrast discrimination performance is constrained by the  
54 nonlinearity that maps physical contrast to neural response, and the intrinsic variability of the  
55 neural representation ('internal noise'). Psychophysical, neurophysiological and  
56 neuroimaging work have converged on a nonlinearity that is expansive at low contrasts and  
57 compressive at higher contrasts (Boynton et al., 1999; Busse, Wade, & Carandini, 2009; Legge  
58 & Foley, 1980). However, there is substantially less agreement regarding the details of  
59 performance-limiting internal noise.

60

61 Most psychophysical models make the assumption that the dominant source of noise for  
62 contrast discrimination is additive (i.e. independent of signal strength) and impacts at a late  
63 stage of processing. The primary justification for this arrangement is the observation that a  
64 dominant source of noise occurring before a nonlinearity will neutralise the effects of that  
65 nonlinearity, rendering it invisible to inspection (termed Birdsall's theorem; Klein & Levi,  
66 2009; Smith & Swift, 1985). Since contrast transduction is observably nonlinear (Boynton et  
67 al., 1999; Busse et al., 2009; Legge & Foley, 1980), any early sources of noise must be  
68 negligible in comparison to the magnitude of late additive noise.

69

70 On the other hand, most electrophysiological and neuroimaging studies have suggested that  
71 perceptually relevant noise is located in early sensory areas (Campbell & Kulikowski, 1972;  
72 Carandini, 2004; Roelfsema & Spekreijse, 2001). Ress and Heeger (2003) demonstrated the  
73 influence of early sensory noise by measuring fMRI blood-oxygen-level dependent (BOLD)  
74 responses in areas V1-V4 during contrast detection. They found that *false alarms* (trials on  
75 which the stimulus was absent, but reported as seen) evoked higher responses than *misses*,  
76 (trials on which the stimulus was present, but reported as not seen) suggesting that these  
77 areas encoded conscious percepts of the stimuli rather than the presence of the stimulus  
78 itself. The origin of the spurious activity in the case of *false alarms* is presumably neural noise  
79 in these early areas. Similarly, several intracranial primate electrophysiology studies have  
80 been able to predict the perceptual decisions of monkeys from neural activity recorded in  
81 early visual areas (Britten, Newsome, Shadlen, Celebrini, & Movshon, 1996; Britten, Shadlen,  
82 Newsome, & Movshon, 1992; Michelson, Pillow, & Seidemann, 2017). This suggests that  
83 sensory decisions are influenced by neural noise at an early stage of processing.

84

85 In this study, we attempt to understand how neural activity governs observer responses in a  
86 two-interval-forced-choice (2IFC) contrast discrimination paradigm, using methods typical of  
87 such studies. Two stimuli are presented in a random order, one containing a 'pedestal' of a

88 fixed contrast (here 50%), and the other containing the pedestal plus a ‘target’ contrast  
89 increment. This paradigm involves several complicating factors that must be considered,  
90 including: (i) the observer must retain a neural representation of the first stimulus for  
91 comparison with the second stimulus, (ii) individuals might have idiosyncratic biases to prefer  
92 one or other interval, and (iii) fast acting adaptation (often termed repetition suppression)  
93 effects might reduce the neural response to the second stimulus (and perhaps also its  
94 appearance). We recorded evoked responses using both EEG (Experiment 1) and MEG  
95 (Experiment 2). We perform traditional univariate analyses, and also employ multivariate  
96 pattern analysis to decode participants’ percepts. Advantages of pattern analysis are that it  
97 can detect subtle and complex effects that might be missed by univariate analyses, is  
98 expressed in meaningful units (classifier decoding accuracy), and permits testing of pattern  
99 generalisation across conditions and time (King & Dehaene, 2014). The high temporal  
100 resolution (~1ms) of electromagnetic recording techniques enabled us to closely examine the  
101 timecourse of perceptual decision making, and the spatial resolution of MEG source space  
102 allowed us to investigate the involvement of discrete anatomical brain areas.

103

104 Our primary motivation was to determine whether the dominant source of neural noise is  
105 located in early sensory brain areas, or later (more frontal) areas involved in making decisions.  
106 To achieve this, our most crucial experimental condition is one in which the target contrast  
107 increment is 0%, meaning that the two stimuli to be compared contain only the pedestal and  
108 are therefore physically identical. Any differences in the neural representation that  
109 correspond to perceptual decisions must be due to processes occurring within the  
110 participant’s nervous system, rather than due to differences in the stimulus. We also included  
111 conditions in which the target contrast was >0% in order to measure psychophysical accuracy,  
112 to keep participants motivated, and to provide information on the timecourse of contrast  
113 discrimination when physical stimuli differ.

114

## 115 **2 Methods**

116

### 117 *2.1 Participants*

118

119 Twenty-two adults with normal or corrected-to-normal vision took part in Experiment 1 and  
120 ten took part in Experiment 2. All participants gave written informed consent. Experiment 1  
121 was approved by the Ethics Committee of the Department of Psychology at the University of  
122 York, and Experiment 2 was approved by the York Neuroimaging Centre Ethics Committee.

123

### 124 *2.2 Stimuli and psychophysical task*

125

126 Stimuli were horizontally oriented sine wave gratings with a spatial frequency of 1c/deg and  
127 a diameter of 10 degrees. The edges of the gratings were blurred by a cosine function. On  
128 each trial, two stimuli were presented: a pedestal stimulus of 50% contrast (where percent  
129 contrast is defined as  $100 * (L_{max} - L_{min}) / (L_{max} + L_{min})$ , where  $L$  is luminance), and a  
130 pedestal+target stimulus consisting of the 50% contrast pedestal plus a target contrast  
131 increment. Five target contrast conditions were used in Experiment 1: 0% (no target), 2%, 4%,  
132 8% and 16%. In Experiment 2 only the 0% (no target) and 16% target contrast conditions were  
133 used. Note that in the ‘no target’ conditions, the stimuli displayed were physically identical

134 and the ‘target’ interval assignment was arbitrary. Participants were not informed of this, and  
135 still made a judgement about which interval appeared higher in contrast.

136

137 The two stimuli on each trial were presented sequentially for 100ms each, with a random  
138 inter-stimulus interval between 400ms and 600ms. The inter-trial interval followed the  
139 participant’s response, and was of variable length between 1000ms and 1200ms to avoid  
140 distortion of ERP averages (Woldorff, 1993). The order of target and non-target intervals  
141 within trials was counterbalanced. Trials of different target contrasts were intermixed and  
142 the order was randomized. Stimulus onsets and participant responses were recorded on the  
143 M/EEG trace using low-latency digital triggers.

144

### 145 *2.3 EEG data collection*

146

147 Event-related potentials were recorded using an ANT Neuroscan EEG system and a 64-  
148 channel Waveguard cap with electrodes arranged according to the 10/20 system. The ground  
149 electrode was positioned at *AFz*, and a whole head average was used as a reference. Data  
150 were digitised at 1kHz using the *ASALab* software. Stimuli were presented on a ViewPixx  
151 display (VPixx Technologies Inc., Quebec, Canada) running in M16 mode (16-bit luminance  
152 resolution) with a mean luminance of 51cd/m<sup>2</sup> and a refresh rate of 120Hz, using Matlab and  
153 elements of the *Psychophysics Toolbox* (Brainard, 1997; Kleiner, Brainard, & Pelli, 2007; Pelli,  
154 1997). The display was gamma corrected using a Minolta LS110 photometer, fitting the data  
155 with a 4-parameter exponential function, and transforming stimulus intensities using the  
156 inverse of the function to ensure linearity.

157

158 Participants were seated in a darkened room 57cm away from the display. Instructions for  
159 the task were to ‘indicate the grating that appeared higher in contrast’. They were asked to  
160 fixate on a central cross throughout the task and used a mouse to indicate their responses.  
161 There were 200 trials per target contrast (1000 trials total, yielding 2000 stimulus-locked  
162 ERPs). The task was run in 5 blocks of approximately 8 minutes, with short breaks in between.

163

### 164 *2.4 MEG data collection*

165

166 MEG data were recorded using a 4D Neuroimaging Magnes 3600 Whole Head 248 Channel  
167 MEG scanner housed in a purpose-built Faraday cage. The data were recorded at 1017.25Hz,  
168 with 400Hz Bandwidth using a High Pass DC filter. Nine channels were identified as having  
169 failed and were removed from all analyses. The location of the head inside the dewar was  
170 continuously monitored throughout the experiment using 5 position indicator head coils.  
171 Stimuli were presented on an Epson EB-G5900 3LCD projector (refresh rate 60Hz; mean  
172 luminance 160cd/m<sup>2</sup>) with a 2-stop ND filter, using *Psychopy* v1.84 (Peirce, 2007). The  
173 projector was gamma corrected using a Minolta LS110 photometer, fitting the data from each  
174 channel (red, green and blue) with a separate exponential function, and transforming  
175 stimulus intensities using the inverse of the function to ensure linearity.

176

177 Participants were seated in a hydraulic chair in front of the projector screen in a dark room.  
178 Prior to the task the three dimensional shape of the participant’s head was registered using a  
179 Polhemus fast-track headshape digitization system. Five fiducial points were used for this over  
180 two registration rounds. If the distance in location between the first and second round was



181 >2mm, the registration was repeated. When successful, the headshape was then traced and  
182 recorded using a digital wand. This was later coregistered with T1-weighted anatomical MRI  
183 scans of each participant acquired in separate sessions using a 3T GE Signa Excite HDx scanner  
184 (GE Healthcare).

185

186 Participants fixated on a small central cross throughout the task. The experiment was  
187 completed in a single block consisting of 240 trials per contrast condition (480 trials in total,  
188 yielding 960 stimulus-locked ERPs), with a total acquisition duration of around 20 minutes. A  
189 single hand response pad was used to make responses in the experiment.

190

## 191 *2.5 EEG data analysis*

192

193 EEG recordings were bandpass filtered (from 0.1Hz to 30Hz) and then epoched into 1 second-  
194 long windows (200ms before stimulus onset to 800ms after) for each interval of every trial.  
195 Each epoch was then baselined at each electrode independently by subtracting the mean  
196 response over the 200ms preceding stimulus onset. ERPs were then sorted by target/non-  
197 target intervals for stimulus classification analysis and then again by selected/non-selected  
198 intervals for decision classification. No artifact rejection was performed, as we have generally  
199 found in previous studies (e.g. Baker, 2017) that this has no material impact on classification  
200 accuracy when trial numbers are large, stimulus presentations are brief, and participants are  
201 adults (as here).

202

203 To perform univariate analyses, ERPs were averaged across a cluster of 10 posterior  
204 electrodes (Oz, O1, O2, POz, PO3-8), and significance was determined using cluster corrected  
205 paired-samples t-tests across participants (Maris & Oostenveld, 2007). The significance of  
206 each cluster was determined by comparing to a null distribution of summed t-values derived  
207 by randomly permuting the labels of the largest cluster 1000 times. To perform multivariate  
208 analyses, a support vector machine (SVM) was used to classify the data independently at each  
209 sample point (i.e. in 1ms steps). A second stage of normalization was applied at each time-  
210 point and each electrode by subtracting the mean response across all intervals and conditions  
211 for that time/sensor combination. The data were then randomly averaged in five subsets of  
212 40 trials for each category (target/non-target or selected/non-selected), of which four subsets  
213 were used to train the model and one was used to test it. The classifier algorithm creates a  
214 parameter space of all data points and then fits a hyperplane boundary that maximizes the  
215 distances between the support vectors of each category. Classifier accuracy for categorising  
216 the test data was averaged across 1000 repetitions of this analysis (with different random  
217 allocations of trials on each repetition), and was repeated for each target contrast condition.  
218 Timecourses of classifier accuracy were then averaged across participants, and periods of  
219 above-chance performance were determined using the same non-parametric cluster  
220 correction procedure as used in the univariate analyses (Maris & Oostenveld, 2007).

221

## 222 *2.6 MEG data analysis*

223

224 Cortical reconstruction and volumetric segmentation was performed with the *Freesurfer*  
225 image analysis suite (<http://surfer.nmr.mgh.harvard.edu/>) using each individual participant's  
226 anatomical MRI scan. Initial MEG analyses were then performed in *Brainstorm* (Tadel, Baillet,  
227 Mosher, Pantazis, & Leahy, 2011). First the MEG sensor array was aligned with the anatomical

228 model of the participant's head using an automated error minimisation procedure.  
229 Covariance matrices were estimated from the data, and a head model comprising overlapping  
230 spheres was generated. A minimum norm solution was used to calculate a source model, with  
231 dipole orientations constrained to be orthogonal to the cortical surface. The model consisted  
232 of a set of linear weights at each location on the cortical surface that transformed the sensor  
233 space representation into source space.

234  
235 MEG data were then imported into Matlab using *Fieldtrip* (Oostenveld, Fries, Maris, &  
236 Schoffelen, 2011), bandpass filtered (from 0.1Hz to 30Hz) and epoched. Univariate and  
237 multivariate analyses were performed in the same way as described for the EEG data in  
238 section 2.5. This was done using the sensor space representation (with 239 working sensors),  
239 the source space representation at approximately 500 vertices evenly spaced across the  
240 cortical mesh, and also within discrete regions of cortex defined by the Mindboggle atlas  
241 (Klein et al., 2017). For this latter analysis, the mean number of vertices in each cortical region  
242 is given in Table A1 in the Appendix. We conducted further analyses using multiple time-  
243 points as observations, at a single spatial (sensor or cortical) location.

244

### 245 **3 Results**

246

#### 247 *3.1 Experiment 1: EEG reveals above-chance classification of percepts*

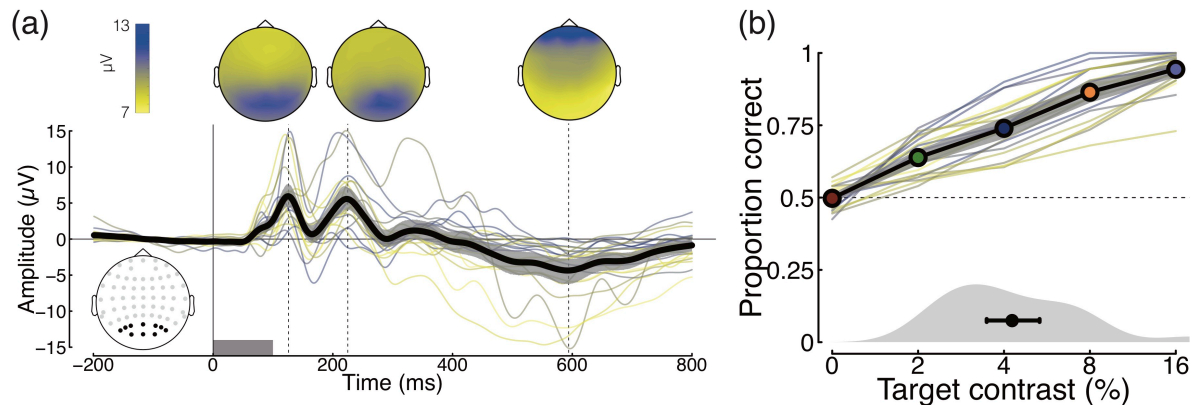
248

249 Mean event-related potentials (ERPs), averaged over the ten occipital electrodes where the  
250 changes in response from baseline were greatest (Figure 1a), showed a typical response to  
251 brief visual stimulation (black curve, Figure 1a). Clear ERPs were evident for all individual  
252 participants (thin traces, Figure 1a). In the grand average (black curve), two successive  
253 positive responses were evident over occipital electrodes at early time-points (126ms and  
254 225ms after stimulus onset), corresponding to stimulus onset and offset. A later time-point  
255 (594ms after stimulus onset) showed negative voltages in occipital areas and positive voltages  
256 in frontal electrodes (see upper headplots for voltage distributions).

257

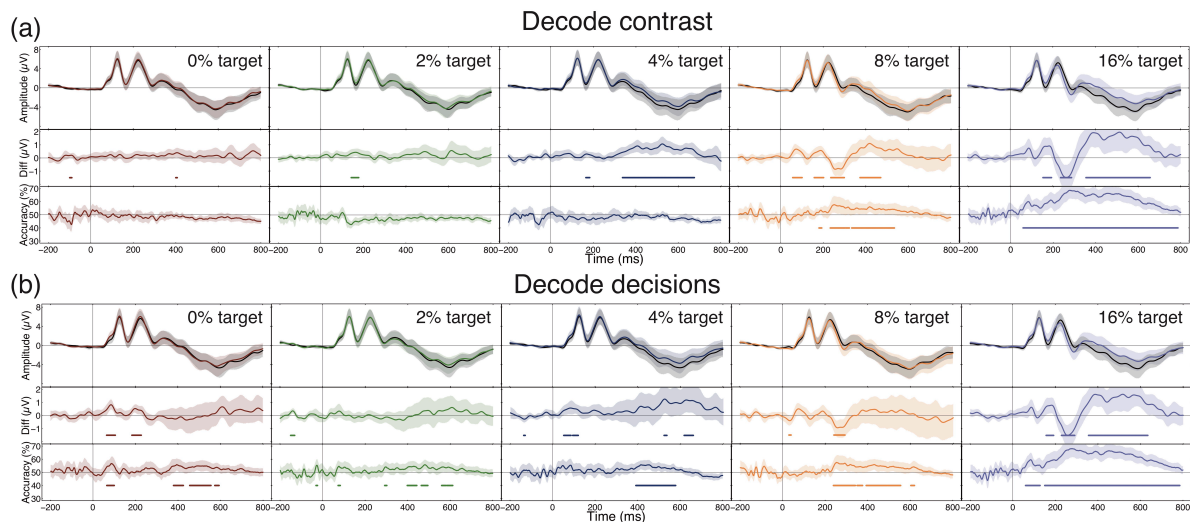
258 Task performance in the five target contrast conditions ranged from chance in the 0% target  
259 contrast condition (where there was no correct answer as the 'target' interval was  
260 determined arbitrarily) to close to ceiling in the 16% target contrast condition (94% correct).  
261 Average data (black line) and results for individual participants (thin traces) are shown in  
262 Figure 1b, where it is evident that increasing target contrast improved performance for all  
263 participants. We fitted cumulative Gaussian functions to each participant's data to estimate  
264 threshold contrast at 75% correct. The mean threshold was 4.25%, with the distribution  
265 shown at the lower axis of Figure 1b.

266



267  
268  
269 Figure 1: Grand mean ERPs (a) and summary of psychophysical performance (b). The black trace in panel (a)  
270 shows the grand mean across all conditions and participants (N=22, with 2000 ERPs per participant), with the  
271 grey shaded region giving 95% confidence intervals derived from 10000 bootstrap resamples. Thinner coloured  
272 traces show results for individual participants. In all cases the evoked responses were averaged across the 10  
273 posterior electrodes shown in the lower left inset. The grey rectangle along the lower axis indicates the period  
274 during which the stimulus was presented. Scalp distributions of voltages at three time points (126ms, 225ms  
275 and 594ms, marked by dashed vertical lines) are shown at the top of the plot. The black line and coloured  
276 symbols in panel (b) show the mean psychophysical performance in each condition, averaged across participants  
277 (N=22), with the grey shaded region giving 95% confidence intervals derived by bootstrapping. Thinner coloured  
278 traces show results for individual participants, and symbol colour corresponds to those used to indicate target  
279 contrast conditions in subsequent figures. The grey curve at the foot shows the distribution of individual  
280 thresholds at the 75% correct point, with the black circle giving the mean, and error bars giving 95% confidence  
281 intervals.

282 We first divided ERP data by contrast, and compared evoked responses in the null (pedestal  
283 only) and target (pedestal + target) intervals. The upper row of Figure 2a shows the ERPs  
284 averaged across occipital electrodes, with the null interval responses shown in black, and the  
285 target interval responses in colour. The middle row of Figure 2a shows the differences  
286 between these two ERPs, with horizontal lines at  $y=-1.5$  indicating time points showing  
287 cluster-corrected significant differences. For a target contrast of 0%, the two stimuli are  
288 identical, and there are no meaningful differences between the waveforms (the two brief  
289 periods of significance are type I errors by definition). As target contrast increases, significant  
290 differences emerge between 100ms and 700ms post stimulus onset. These likely reflect both  
291 differences in early evoked responses, and also later decision-related components.  
292 Multivariate analyses across all 64 electrodes showed significant decoding only at the highest  
293 two target contrast levels (lower row of Figure 2a) within the same time window.

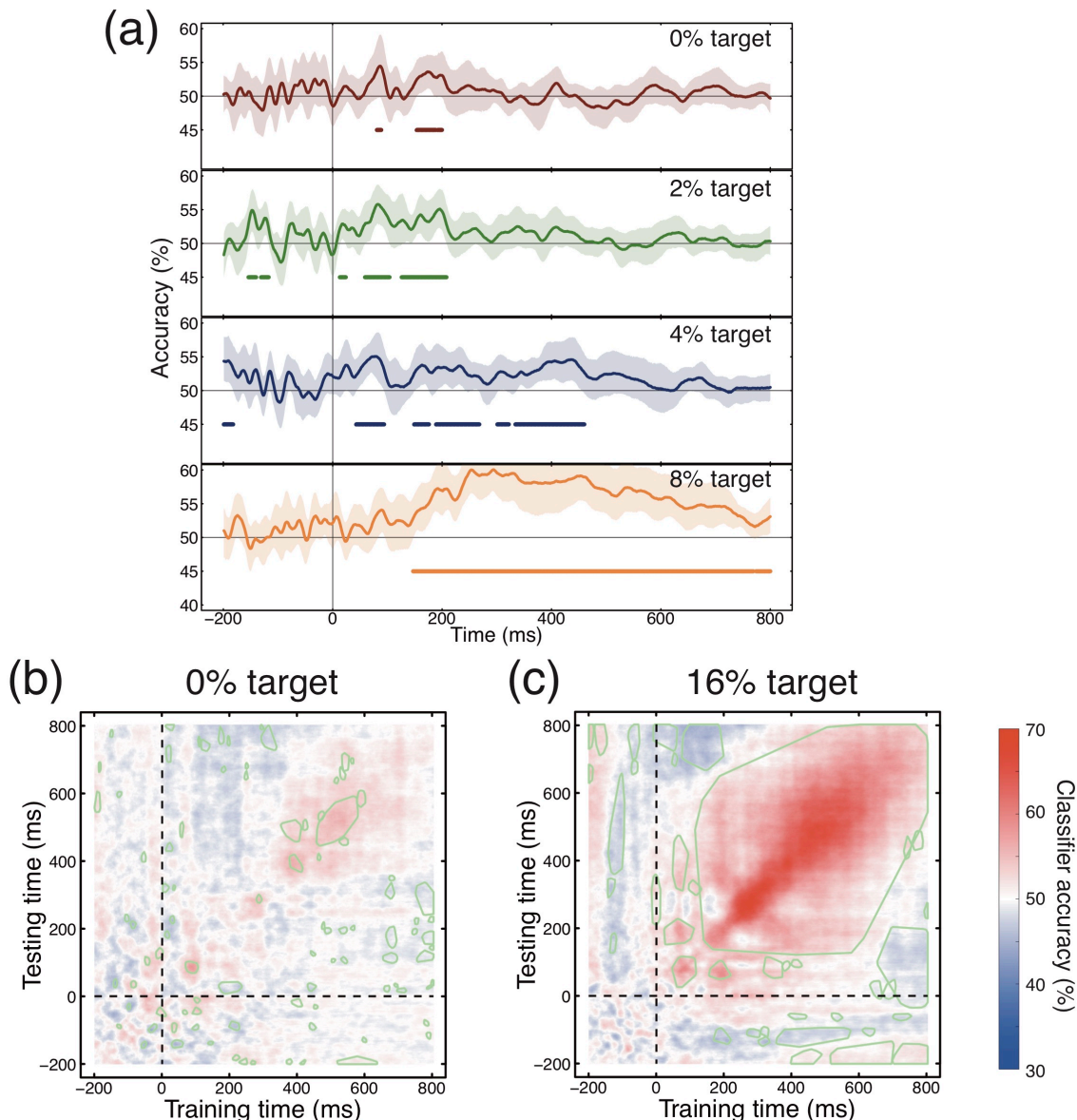


294  
295 Figure 2: Univariate and multivariate analyses of EEG data. Panel (a) shows results for data partitioned according to the stimulus contrast (pedestal vs pedestal+target), and panel (b) shows results for data partitioned according to the participants' perceptual decisions (selected vs non-selected). The upper section of each sub-plot contains  
296 grand averages of the ERPs being compared, in which the coloured curve indicates the target (or selected)  
297 waveform, and the black curve indicates the pedestal (or non-selected) waveform. The middle section of each  
298 sub-plot is the difference waveform. The lower section of each sub-plot shows multivariate classifier  
299 performance at each timepoint, where the baseline is 50% correct. In each panel, shaded regions show 95%  
300 confidence intervals across participants (N=22), calculated by bootstrapping. The coloured horizontal lines in the  
301 lower two sections indicate periods of time when the difference waveforms were significantly different from 0  
302 (middle plots) or exceeded 50% correct (lower plots), calculated using a nonparametric cluster correction  
303 procedure (Maris & Oostenveld, 2007).  
304  
305

306  
307 Next, we repeated the analyses on the same data, but this time organised according to the  
308 participant's decisions rather than the physical stimulus contrast. In other words, we took  
309 ERPs from the intervals selected by the participants as appearing higher in contrast, and  
310 compared these with ERPs from the non-selected intervals. This analysis revealed additional  
311 time periods where the ERPs were significantly different, particularly in the 0% target  
312 condition, where differences were observed at around 100ms post stimulus onset. This  
313 finding was echoed in the multivariate analyses, which showed above chance decoding at  
314 early time points (around 100ms), as well as a sustained period of above chance decoding at  
315 all target contrasts from around 400-600ms post stimulus onset. The 0% target condition is  
316 of particular interest for this analysis, as any differences between evoked responses are not  
317 determined by the stimulus (which is identical in both intervals), and must be a consequence  
318 of differences in neural activity. The early significant clusters in both univariate and  
319 multivariate analyses indicate differences in the amplitude of the evoked response that  
320 influence subsequent perceptual decisions. Higher target contrasts increasingly converge  
321 with the contrast decoding analysis, as performance approaches ceiling (see Figure 1b) and  
322 the majority of selected intervals also contained the target (e.g. results for the 16% target  
323 condition are near identical in Figure 2a,b).  
324

325 We tested the generality of the multivariate results in two ways. First, we took the classifier  
326 trained to discriminate between perceptual decisions at the highest target contrast (16%),  
327 and used this model to predict performance at lower target contrasts. This analysis (shown in  
328 Figure 3a) replicates the early periods of above chance decoding for 0% target contrast trials,  
329 suggesting that observers use a similar decision strategy for very challenging discriminations

330 as for easier ones. Next, we took the classifier trained at each time point, and used it to predict  
331 selected and non-selected trials at all other time points (King & Dehaene, 2014). The results  
332 of this temporal generalization analysis (shown in Figure 3b,c) reveal isolated early structures  
333 around 100ms and 200ms, and a more sustained pattern from 400-600ms (in the 0%  
334 condition) and from 200-800ms (in the 16% condition). We propose (see Discussion) that the  
335 early periods of above chance decoding may represent neural noise at the initial stages of  
336 processing, and the later periods could reflect noise in perceptual decisions or memory traces  
337 from the first temporal interval.  
338



339 Figure 3: Multivariate generalization analyses across contrast condition (a) and time (b,c), for data partitioned  
340 according to the participants' perceptual decisions. Panel (a) shows classifier accuracy at the four lower target  
341 contrasts after training the algorithm at the highest target contrast. Plotting conventions are as described for  
342 the multivariate analyses shown in Figure 2. Panels (b,c) show classifier accuracy when trained at each time  
343 point independently, and then tested using data at all time points. Regions enclosed by green lines indicate  
344 clusters where classifier accuracy differed significantly from chance (50% correct).  
345

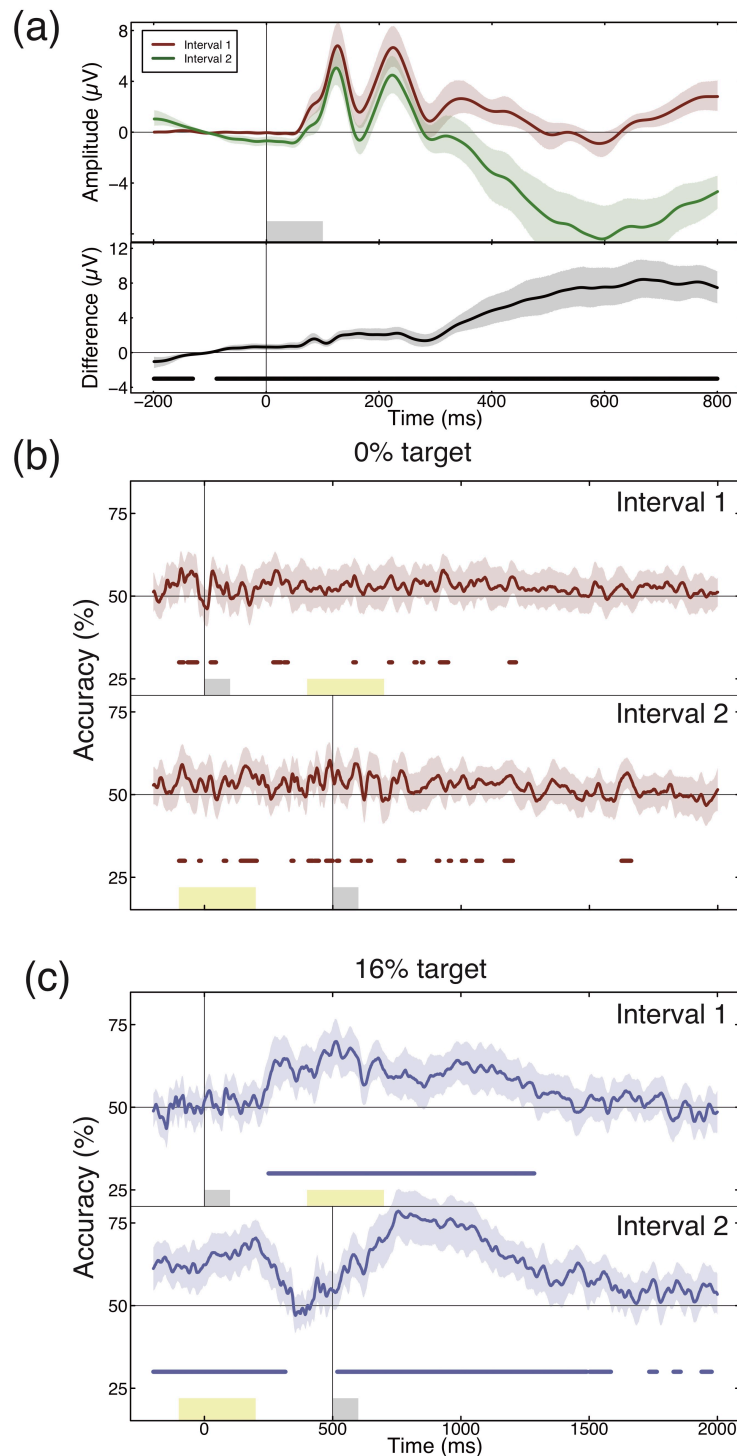
346

### 347 *3.2 Interval biases and decoding within the first or second interval*



348

349 The temporal structure of a 2IFC trial is necessarily asymmetric, as the observer has  
350 knowledge of the first interval by the time they experience the second interval. In addition,  
351 repetition suppression effects can affect the evoked amplitude of the second presentation  
352 (Grill-Spector, Henson, & Martin, 2006). We first compared the average ERPs for all pedestal-  
353 only presentations (where the stimulus contrast was 50%) across the two intervals. We find  
354 both subtle and gross differences between these waveforms (see Figure 4a). Before stimulus  
355 onset, the waveforms differ as the second interval (green trace) has a decreasing voltage  
356



357



358 Figure 4: Comparisons across trial intervals. Panel (a) shows evoked responses in the first (red curve) and second  
359 (green curve) intervals of a 2IFC trial (upper plot) and their difference (lower plot). The evoked response is  
360 generally more negative in the second interval, particularly at time points >250ms after stimulus onset, despite  
361 the contrasts being physically identical (both 50%). Panels (b,c) show multivariate pattern classifier accuracy  
362 when comparing evoked potentials time-locked to either the first interval (upper plots) or the second interval  
363 (lower plots), for target contrasts of 0% (panel b) or 16% (panel c). In each plot, the shaded grey region shows  
364 the presentation of the stimulus from that interval and the yellow shaded region shows the range of time points  
365 when the stimulus from the other interval was presented (the precise inter-stimulus interval was jittered on  
366 each trial to reduce entrainment of ERP averages). In all panels shaded regions around each curve show 95%  
367 confidence intervals across participants, and horizontal coloured lines indicate significant clusters, consistent  
368 with conventions in previous figures.

369

370 during the 200ms before the stimulus is presented. This likely originates from the tail end of  
371 the evoked response from the first interval (see Woldorff, 1993), which is decreasing from  
372 400-600ms (the time window in which the second interval occurred). The second interval then  
373 has a more generally negative voltage throughout the 800ms following stimulus onset. The  
374 magnitude of this difference is much greater than that at stimulus onset, and so would persist  
375 even with a different baseline normalization regime (e.g. if the voltages were normalized to  
376 those at  $t=0$ ). Furthermore, the differences become much more substantial at later time  
377 points, from 400-800ms. This may relate to the perceptual decision and motor response that  
378 the participant must make following the second interval.

379

380 Do these substantial differences in the evoked response to two physically identical stimuli  
381 affect the observer's perception of the stimulus, or their decision over which interval to  
382 choose? We estimated interval bias for all participants by calculating the proportion of trials  
383 on which the second interval was selected, for the 200 trials in the 0% target contrast  
384 condition (where the two stimuli are identical). If this index is significantly below 0.5, it  
385 indicates a bias towards the first interval, and if it is significantly above 0.5 it indicates a bias  
386 towards the second interval. Despite individuals showing idiosyncratic biases (indices ranged  
387 from 0.23 to 0.92), the mean bias index was precisely 0.5 (SD: 0.14) and not significantly  
388 different from it ( $t_{21}=0.11$ ,  $p=0.91$ ). The substantial voltage differences (Figure 4a) therefore  
389 do not appear to reflect group level differences in the appearance of the stimuli across  
390 intervals, and any idiosyncratic biases would presumably only reduce the power of our  
391 decision-based decoding analyses (Figure 2b), which are nevertheless significant.

392

393 The size of the voltage differences across intervals prompted us to investigate the extent to  
394 which decisions can be decoded within one or other interval, making comparisons across  
395 trials (within an interval) instead of across intervals (within a trial). The finite number of trials,  
396 combined with the presence of interval biases for some observers (see above) meant that  
397 there were often different numbers of trials available in the two intervals, so it was necessary  
398 to train and test the classifier on averages of fewer than 40 trials in some cases. The results  
399 of this multivariate analysis are shown in Figure 4b/c for decoding perceptual decisions at 0%  
400 contrast (Fig 4b) and at 16% contrast (Fig 4c), and for all conditions in Figure A1. In each sub-  
401 plot, the upper trace shows the classifier performance for data from interval 1 (with ERPs  
402 aligned at  $t=0$ ms), and the lower trace shows the classifier performance for data from interval  
403 2 (with ERPs aligned at  $t=500$ ms). The yellow shaded regions indicate the time window when  
404 the stimulus in the other interval was displayed (the jittered inter-stimulus interval means  
405 that this time window is probabilistic rather than exact). Overall, we find increased decoding

406 accuracy in the second interval compared with the first. This presumably reflects the  
407 increased information available for making a decision following the second stimulus.

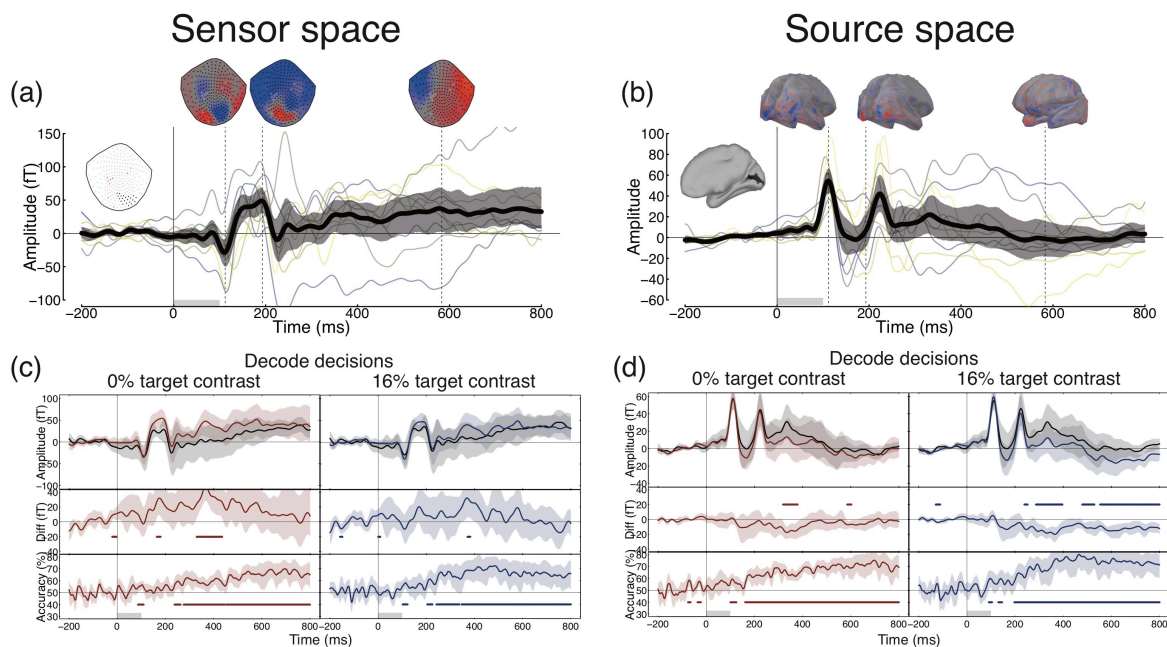
408

### 409 3.3 Experiment 2: source space decoding is more sensitive than sensor space decoding

410

411 We confirmed that our MEG data replicated the key effects from Experiment 1 in several  
412 ways. First, we performed univariate and multivariate analyses in sensor space, using a cluster  
413 of posterior sensors for the univariate analysis, and all working sensors (N=239) for the  
414 multivariate analysis. The results of this analysis are shown in Figure 5a,c for the data split by  
415 participants' perceptual decisions. Consistent with the EEG results, we find above chance  
416 pattern classification at early time points (~100ms) as well as later >200ms. Second, we  
417 performed complementary analyses in MEG source space, using ERPs from pericalcarine  
418 cortex (corresponding to early visual cortex) for the univariate analyses, and a subset of 500  
419 vertices across the entire cortical surface for the multivariate analyses. The results of this  
420 analysis are shown in Figure 5b,d. The general pattern of results is consistent with the sensor  
421 space analysis, though the shape of the ERP waveforms from pericalcarine cortex is somewhat  
422 different from those recorded in sensor space, with the peaks of the onset and offset  
423 response appearing more prominent, and the response returning to baseline by around  
424 500ms. Interestingly, we found that the multivariate analysis produced greater classification  
425 accuracy in source space (maximum of 80% correct) versus sensor space (maximum of 72%  
426 correct). We discuss possible reasons for this in the Discussion. Having confirmed that the  
427 multivariate source space analysis can decode perceived contrast, we next asked which brain  
428 regions contained information relevant to the task.

429



430

431 Figure 5: Sensor space and source space MEG analysis. Panel (a) shows the grand average ERP for all conditions  
432 and participants, pooled across a subset of MEG sensors indicated in black in the leftmost inset. Magnetic field  
433 distributions across the sensor array are shown at three time points at the top of the plot. Panel (b) shows a  
434 similar analysis in source space, for a region of cortex around the calcarine sulcus (highlighted black in the  
435 leftmost inset). The evoked response at each vertex on the cortical mesh was normalised such that the 110ms  
436 deflection was always positive, to avoid signal cancellation due to polarity inversions. In both panels, thin  
437 coloured curves represent individual participants (N=10). Panels (c,d) show univariate and multivariate  
438 comparisons between selected and non-selected ERPs in both contrast conditions, in the same format as

439 described for Figure 2. Panel (c) shows this analysis in sensor space, and panel (d) shows the same analysis in  
440 source space. The source space multivariate analyses used a matrix of around 500 points distributed across the  
441 surface of the cortex.

442

### 443 *3.4 Classification in anatomically-defined brain regions*

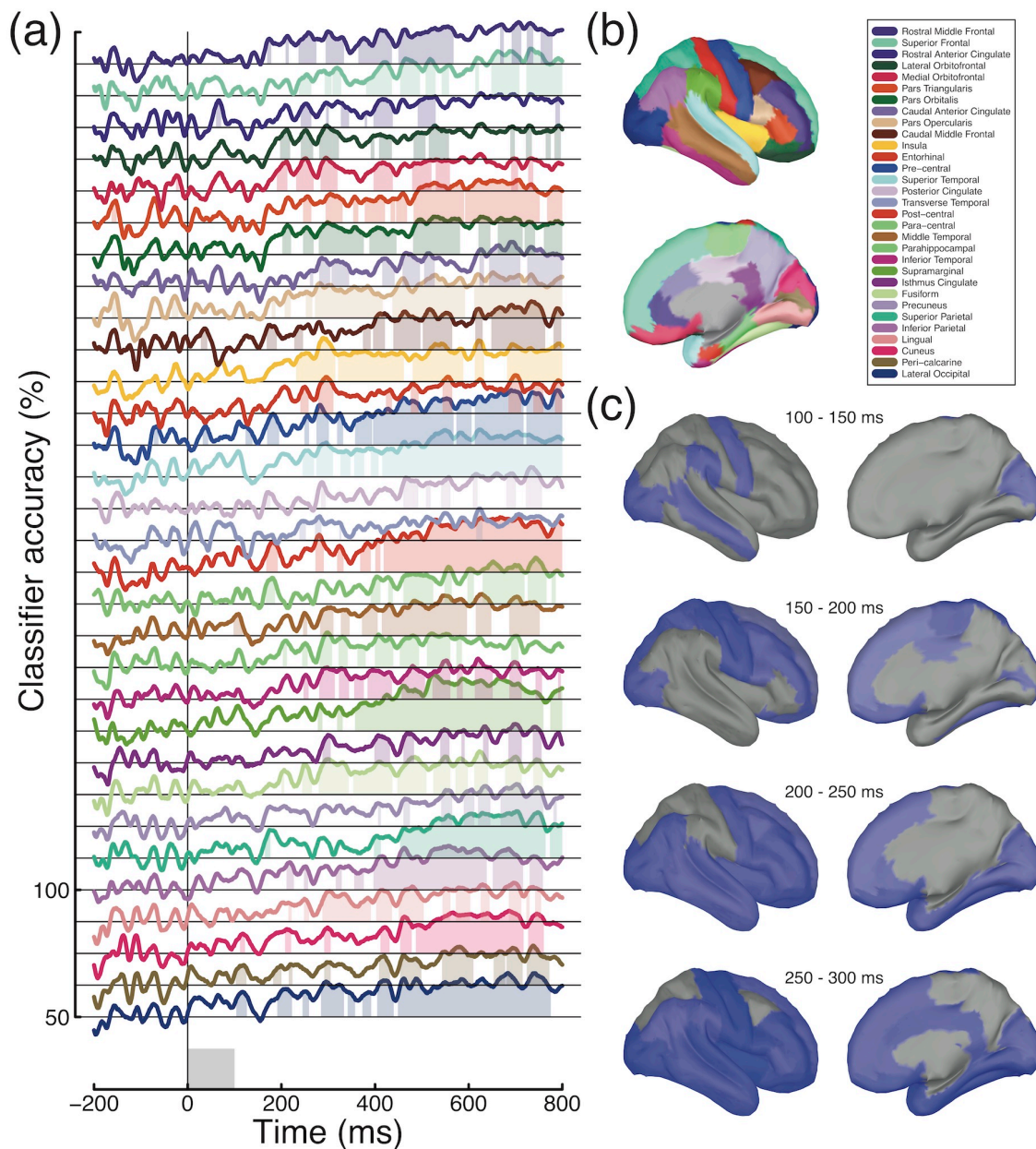
444

445 We divided the cortex into 31 discrete non-overlapping anatomical regions using the  
446 *Mindboggle* atlas (Klein et al., 2017). Maximal evoked potentials in these regions showed  
447 clear differentiation (see Figure A2). Because regions differed in size, each area contributed a  
448 different number of vertices on the cortical mesh for pattern classification (see Table A1).

449

450 At early time points, around 100ms, information in three adjacent regions around the  
451 occipital pole (the peri-calcarine region, the cuneus and the lateral occipital cortex) could be  
452 used to decode the participant's percept in the 0% target contrast condition (final three traces  
453 in Figure 6a). Over time, this information spread forward to frontal and temporal cortex (see  
454 Figure 6c). By 300ms following stimulus onset, almost the entire brain contains information  
455 relevant to the task. This includes regions that do not appear to respond directly to  
456 presentation of visual stimuli (i.e. where there is no obvious evoked response, see Figure A2).  
457 A similar pattern of results is evident in the 16% target contrast condition (see Figure A3),  
458 confirming our earlier finding that differences in physical and perceived contrast are  
459 processed in a similar fashion.

460



461  
 462 Figure 6: Atlas-based classification of decisions in the 0% target condition. Timecourses in panel (a) indicate  
 463 classifier performance for each brain region, offset vertically for clarity, and organised from anterior (top) to  
 464 posterior (bottom) (see legend in panel b). Shaded regions in panel (a) indicate clusters in which classification  
 465 performance was significantly above chance (Bonferroni corrected for 31 brain regions). In panel (c), regions  
 466 containing significant clusters within a given time window are shown in blue.

467

#### 468 **4 Discussion**

469

470 The present study investigated the timecourse and location of perceptually relevant neural  
 471 noise in contrast discrimination, using univariate and multivariate analysis of EEG and MEG  
 472 data. Our results show that perceptual decisions are partly determined by responses in early  
 473 visual cortex even when the two stimuli in a discrimination task are physically identical. This  
 474 indicates that perceptually relevant neural noise impacts at the initial stages of processing  
 475 and affects stimulus encoding in the visual system. However the best classifier performance  
 476 occurred at later time points (>400ms), suggesting that additional sources of noise might also  
 477 be involved. Analysis of differences across trial intervals revealed that neural activity in the



478 second interval was more closely associated with subsequent decisions. We will now discuss  
479 the implications of these finding for our understanding of how neural activity (both evoked  
480 and spontaneous) influences the perceptual decisions involved in sensory discrimination.

481

#### 482 *4.1 Superior classification in MEG source space*

483

484 Classifier performance overall was much higher for MEG data than for EEG data in identical  
485 conditions, despite the larger sample size of the EEG study (N=22 for EEG vs. N=10 for MEG).  
486 This is presumably due to the greater intrinsic sensitivity of MEG sensors, and the greater  
487 sampling density across the scalp (N=64 for EEG vs. N=239 for MEG). Classifier accuracy was  
488 also consistently higher in source space than in the sensor space representation primarily  
489 used in previous MEG studies (Cichy, Pantazis, & Oliva, 2014; Clarke, Devereux, Randall, &  
490 Tyler, 2015; Mostert, Kok, & de Lange, 2016). Since the source space representation is a  
491 weighted linear combination of activity at the sensors, this might be somewhat surprising.  
492 However, the source reconstruction presumably weights out signals from outside the brain  
493 (e.g. heart rate, breathing and blinking artefacts, and noise from outside of the scanner),  
494 resulting in a cleaner signal. Some form of source localisation may therefore be a useful  
495 processing step in future studies attempting multivariate classification of MEG signals.  
496 Additionally, combining the source space representation with atlas-based multivariate  
497 analysis permits questions to be asked about the information contained in specific brain  
498 regions at different points in time.

499

#### 500 *4.2 Single interval versus 2IFC*

501

502 One distinction between this and most previous studies on the neural correlates of perceptual  
503 decision making is that previous work has used single interval (yes/no) paradigms  
504 (Hesselmann, Kell, Eger, & Kleinschmidt, 2008; Hillyard, Squires, Bauer, & Lindsay, 1971; Jolij,  
505 Meurs, & Haitel, 2011; Mostert et al., 2016; Ress & Heeger, 2003; Schölvinc, Friston, & Rees,  
506 2012; Squires, Squires, & Hillyard, 1975), whereas here we used a 2IFC design. Since most  
507 psychophysical studies of contrast discrimination have used 2IFC, this choice has direct  
508 relevance to previous work. Additional benefits are that the number of evoked potentials in  
509 the selected and non-selected categories were necessarily balanced, and it was possible to  
510 analyse perceptual decisions based on two physically identical stimuli. In addition, 2IFC  
511 designs avoid problems with differences in bias (or response criteria) between participants,  
512 as pairs of stimuli are compared directly on a given trial (rather than against an internal  
513 standard). However, 2IFC cannot distinguish between hits and correct rejections (as these  
514 comprise 'correct' trials) or between misses and false alarms (incorrect trials), so direct  
515 comparisons of these trial categories is not possible in our design.

516

517 Another feature of 2IFC paradigms is that participants must hold information about the  
518 stimulus from the first interval in memory until after the second stimulus has been presented.  
519 This process may account for the sustained patterns of activity that permit classification long  
520 after stimulus presentation (see Figures 2-6). In particular, our analysis of interval-specific  
521 effects (see Figure 4b,c) shows greater multivariate decoding accuracy in the second interval,  
522 presumably because at this point in the trial the observer has obtained all information  
523 necessary to make a decision.

524

#### 525 4.3 *Multiplicative noise*

526

527 An alternative account of contrast discrimination performance at high pedestal contrasts is  
528 that transduction is linear but internal noise is signal-dependent (Pelli, 1985). If the dominant  
529 source of noise were early and multiplicative, this would avoid any issues relating to Birdsall's  
530 theorem, as the transducer could be linear. It has proven difficult to distinguish between the  
531 multiplicative and additive noise accounts purely from contrast discrimination experiments  
532 (Georgeson & Meese, 2006; Kontsevich, Chen, & Tyler, 2002). At a single neuron level there  
533 is well-established evidence of multiplicative noise (Tolhurst, Movshon, & Dean, 1983), yet it  
534 appears that across populations of neurons with different sensitivities the overall noise is  
535 effectively additive (Chen, Geisler, & Seidemann, 2006). Since evidence from fMRI (Boynton  
536 et al., 1999), EEG (Busse et al., 2009) and psychophysics (Kingdom, 2016) all argue strongly  
537 against a linear transducer, we think this explanation is unlikely to account for the body of  
538 available data.

539

#### 540 4.4 *Resolving early noise and Birdsall's theorem*

541

542 Early noise has typically been considered at very early stages, including photoreceptor noise  
543 in the retina (Barlow, 1962), which can be considered as external noise (albeit in a different  
544 sense from experimentally added external noise, as it is not under the direct control of the  
545 experimenter). Late additive noise is often assumed (either implicitly or explicitly) to be added  
546 at the decision stage, long after the nonlinearities of early visual processing (Cabrera, Lu, &  
547 Doshier, 2015; Mueller & Weidemann, 2008). The results here point to a perceptually-relevant  
548 source of noise that is present in the early evoked response, at around 100ms or earlier.  
549 However we find that classification performance improves after this point in processing,  
550 reaching a maximum around 700ms after target onset (see Figure 3e). In addition, our  
551 temporal generalisation analysis (see Figure 3b,c) shows that these two time windows involve  
552 distinct patterns of electrical activity, implying separate sources of noise. This is consistent  
553 with a sequence of multiple (and presumably independent) noise sources at different stages  
554 of processing. Since mathematical treatment of complex systems involving multiple  
555 nonlinearities and noise sources is currently lacking, it is unclear what implications this would  
556 have for the visibility of early nonlinearities.

557

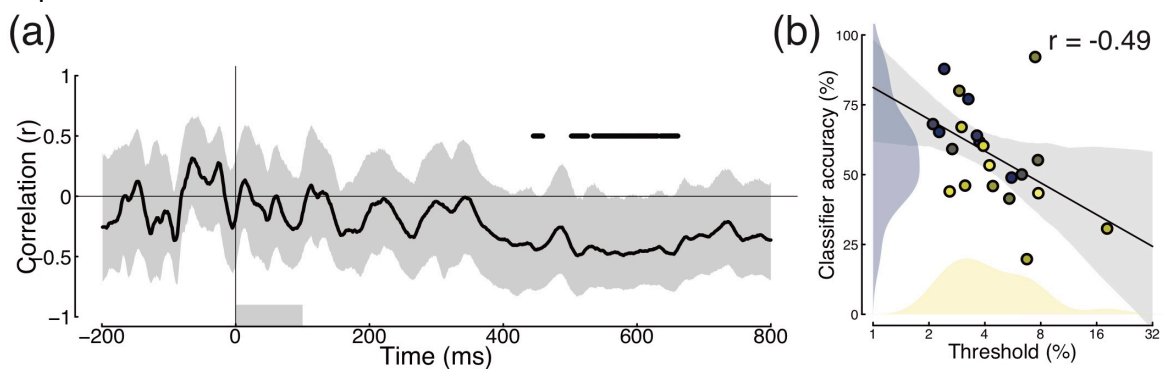
558 One possibility is that a strong source of noise occurs immediately after the initial contrast  
559 transduction nonlinearity in V1, leaving that nonlinearity visible but obscuring later ones. This  
560 would explain why psychophysical contrast perception maps closely onto the neural response  
561 from early visual areas (Baker & Wade, 2017; Barlow, Hawken, Parker, & Kaushal, 1987;  
562 Boynton et al., 1999), but not the highly compressive contrast-invariant response in later  
563 regions (Avidan et al., 2002; Rolls & Baylis, 1986). Indeed, this might enable the visual system  
564 to harness the properties of Birdsall linearisation to preserve the dynamic range of early  
565 representations through later processing (that is more compressive) when making  
566 comparisons across stimuli (as in a discrimination paradigm). Object recognition, and other  
567 operations that benefit from invariance to features such as contrast, position and size, but do  
568 not require comparisons across multiple stimuli, would be immune to the Birdsall effect and  
569 benefit from the later nonlinearities. Furthermore, a strong early source of noise would make  
570 the study of later 'mid-level' visual processes much more challenging, perhaps explaining why



571 vision research has typically focussed on earlier mechanisms and can be caricatured as being  
572 'stuck' in V1 (Graham, 2011; Peirce, 2007).

573

574 In order to investigate these possibilities further, we performed two additional analyses. To  
575 link the internal fluctuations measured in our experiments with a psychophysical measure of  
576 internal noise, we correlated classifier accuracy with the contrast discrimination thresholds  
577 estimated from the psychophysical responses in Experiment 1. Since high internal noise  
578 should result in higher discrimination thresholds (poorer performance), we predicted that the  
579 two measures would be correlated at time points where the neural fluctuations were most  
580 relevant to perception. This analysis is shown in Figure 7, and reveals a time window with  
581 significant negative correlations around 450-650ms (i.e. high thresholds correspond to poor  
582 classifier performance). We speculate that neural noise within this time window most closely  
583 corresponds to the 'late' additive noise that is a feature of contemporary models of contrast  
584 discrimination. However it is also possible that other factors mediate this relationship,  
585 including the interval bias described in the Results section which could inflate negative  
586 correlations by driving thresholds up and classifier performance down. Nevertheless, it is  
587 interesting to demonstrate a link between psychophysical thresholds and decoding of neural  
588 responses.



589

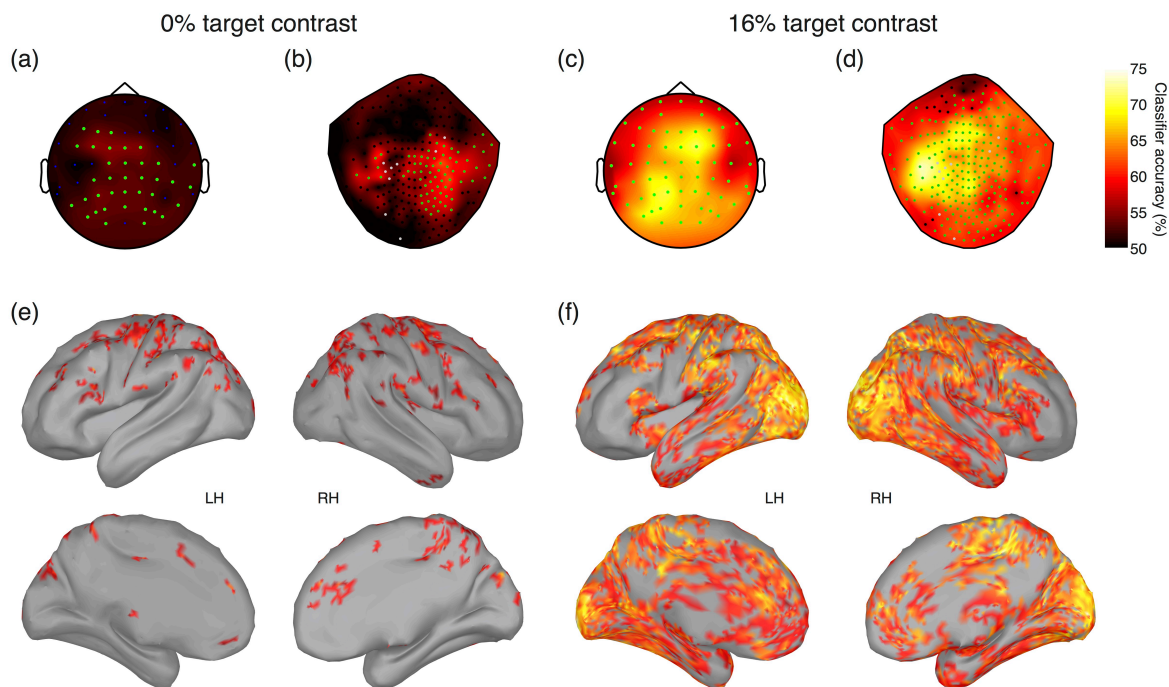
590 Figure 7: Correlation between individual contrast discrimination thresholds (see distribution in Figure 1b) and  
591 classifier accuracy in the 0% target contrast condition of Experiment 1 (N=22). Panel (a) shows the correlation  
592 as a function of time. The horizontal black lines at  $r=0.5$  denote clusters of significant effects (two-tailed),  
593 according to a nonparametric cluster correction procedure (Maris & Oostenveld, 2007). Grey shaded regions  
594 represent bootstrapped 95% confidence intervals calculated across participants, and the lower grey rectangle  
595 shows the period when the stimulus was displayed. To further illustrate this relationship, panel (b) shows a  
596 scatterplot of the correlation between thresholds and the averaged classifier performance within all significant  
597 clusters identified in (a). The diagonal line is the best fitting Deming regression line, with grey shaded regions  
598 showing bootstrapped 95% confidence intervals, and blue and yellow histograms showing the distribution of  
599 values for each measure.

600

601 The final analysis we performed was inspired by the suggestions of an anonymous reviewer,  
602 who pointed out that in our main multivariate analyses, although the classifier is always  
603 trained on information from both trial intervals, test data are supplied from one interval at a  
604 time. This means that the classifier's decisions differ from those of human participants, who  
605 in a 2IFC paradigm always have information available from both trial intervals. We conducted  
606 further multivariate analyses, by training and testing the classifier on downsampled  
607 timecourses of entire 2IFC trials combined across both intervals (to account for the jittered  
608 ISI, each interval was aligned to its respective trigger).

609

610 The results of this analysis are shown in Figure 8 for the EEG experiment (Figure 8a,c), and for  
611 the MEG experiment in both sensor space (Figure 8b,d) and source space (Figure 8e,f). All  
612 data sets produced above-chance classification at some sensors and brain regions, indicating  
613 that patterns across time were able to discriminate neural states. For the 16% target contrast,  
614 early visual areas at the occipital pole showed high classifier accuracy (Figure 8f), consistent  
615 with the salient target contrast increment producing greater ERP amplitudes in the target  
616 interval (see Figures 2 & 5). For the 0% target contrast condition, accuracy in early visual  
617 regions was relatively poor, and the highest accuracy was in fronto-parietal regions (Figure  
618 8e). This suggests that the most important signals for classifying decisions in this condition  
619 arise after the initial responses in visual brain areas. The later sustained response from around  
620 400ms onwards (see Figures 2b & 3b) seems more consistent with the brain regions producing  
621 significant decoding here. These additional analyses suggest that the internal noise sources  
622 most relevant for contrast discrimination performance occur subsequent to the initial visual  
623 cortical responses, and are therefore more consistent with models of 'late' noise than with  
624 early internal (or unintended external) noise.  
625



626  
627 Figure 8: Whole-trial pattern classification accuracy in sensor space and source space. Entire time courses of  
628 both 2IFC intervals were categorised according to participant percepts (selected vs non-selected), and  
629 downsampled in steps of 10ms. Classifier accuracy was averaged across participants at individual electrodes in  
630 the EEG experiment (panels a,c), in sensor space in the MEG experiment (panels b,d) and at 15000 vertices on  
631 the cortical surface in source space in the MEG experiment (panels e,f). Sensors comprising significant clusters  
632 are marked by green points in panels a-d, and vertices not part of significant clusters are coloured grey in panels  
633 e,f.

#### 634 635 4.5 Conclusion

636  
637 To summarise, in this study we investigated the timecourse of the neural operations involved  
638 in contrast discrimination. We demonstrated that internal noise impacting early in time  
639 (around 100ms after stimulus onset) and in the visual pathway can affect sensory processing  
640 and perceptual decisions. However, the strongest internal noise source was later (around

641 400-700ms), involved parietal and frontal brain regions, and was correlated with  
642 psychophysical thresholds. Our novel application of multivariate analysis methods to discrete  
643 spatial regions of MEG source space offers the capability of studying how the brain represents  
644 information in both space and time.

645

## 646 **5 References**

647

648 Avidan, G., Harel, M., Hendler, T., Ben-Bashat, D., Zohary, E., & Malach, R. (2002). Contrast  
649 sensitivity in human visual areas and its relationship to object recognition. *Journal of*  
650 *Neurophysiology*, *87*(6), 3102–3116.

651 Baker, D. H., & Wade, A. R. (2017). Evidence for an Optimal Algorithm Underlying Signal  
652 Combination in Human Visual Cortex. *Cerebral Cortex*, *27*, 254–264.  
653 <http://doi.org/10.1093/cercor/bhw395>

654 Barlow, H. B. (1962). A method of determining the over-all quantum efficiency of visual  
655 discriminations. *The Journal of Physiology*, *160*, 155–168.

656 Barlow, H. B., Hawken, M., Parker, A. J., & Kaushal, T. P. (1987). Human contrast  
657 discrimination and the threshold of cortical neurons. *Journal of the Optical Society of*  
658 *America A*, *4*(12), 2366. <http://doi.org/10.1364/JOSAA.4.002366>

659 Boynton, G. M., Demb, J. B., Glover, G. H., & Heeger, D. J. (1999). Neuronal basis of contrast  
660 discrimination. *Vision Research*, *39*(2), 257–269. [http://doi.org/10.1016/S0042-](http://doi.org/10.1016/S0042-6989(98)00113-8)  
661 [6989\(98\)00113-8](http://doi.org/10.1016/S0042-6989(98)00113-8)

662 Brainard, D. H. (1997). The Psychophysics Toolbox. *Spatial Vision*, *10*, 433–436.

663 Britten, K. H., Newsome, W. T., Shadlen, M. N., Celebrini, S., & Movshon, J. A. (1996). A  
664 relationship between behavioral choice and the visual responses of neurons in macaque  
665 MT. *Visual Neuroscience*, *13*(01), 87–100. <http://doi.org/10.1017/S095252380000715X>

666 Britten, K. H., Shadlen, M. N., Newsome, W. T., & Movshon, J. A. (1992). The analysis of visual  
667 motion: a comparison of neuronal and psychophysical performance. *The Journal of*  
668 *Neuroscience: The Official Journal of the Society for Neuroscience*, *12*(12), 4745–4765.

669 Busse, L., Ayaz, A., Dhruv, N. T., Katzner, S., Saleem, A. B., Scho, M. L., ... Carandini, M. (2011).  
670 The Detection of Visual Contrast in the Behaving Mouse, *31*(31), 11351–11361.  
671 <http://doi.org/10.1523/JNEUROSCI.6689-10.2011>

672 Busse, L., Wade, A. R., & Carandini, M. (2009). Representation of Concurrent Stimuli by  
673 Population Activity in Visual Cortex. *Neuron*, *64*(6), 931–942.  
674 <http://doi.org/10.1016/j.neuron.2009.11.004>

675 Cabrera, C. A., Lu, Z.-L., & Doshier, B. A. (2015). Separating decision and encoding noise in  
676 signal detection tasks. *Psychological Review*, *122*(3), 429–460.  
677 <http://doi.org/10.1037/a0039348>

678 Campbell, F. W., & Kulikowski, J. J. (1972). The visual evoked potential as a function of contrast  
679 of a grating pattern. *The Journal of Physiology*, *222*(2), 345–356.  
680 <http://doi.org/10.1113/jphysiol.1972.sp009801>

681 Carandini, M. (2004). Amplification of trial-to-trial response variability by neurons in visual  
682 cortex. *PLoS Biology*, *2*(9). <http://doi.org/10.1371/journal.pbio.0020264>

683 Chen, Y., Geisler, W. S., & Seidemann, E. (2006). Optimal decoding of correlated neural  
684 population responses in the primate visual cortex. *Nature Neuroscience*, *9*(11), 1412–  
685 1420. <http://doi.org/10.1038/nn1792>

686 Cichy, R. M., Pantazis, D., & Oliva, A. (2014). Resolving human object recognition in space and  
687 time. *Nature Neuroscience*, *17*(3), 455–462. <http://doi.org/10.1038/nn.3635>

- 688 Clarke, A., Devereux, B. J., Randall, B., & Tyler, L. K. (2015). Predicting the Time Course of  
689 Individual Objects with MEG. *Cerebral Cortex*, 25(10), 3602–3612.  
690 <http://doi.org/10.1093/cercor/bhu203>
- 691 Fechner, G. T. (1912). The classical psychologists: Selections illustrating psychology from  
692 Anaxagoras to Wundt. In B. Rand (Ed.), *Elements of psychophysics* (pp. 562–572). Boston:  
693 Houghton Mifflin.
- 694 Georgeson, M. A., & Meese, T. S. (2006). Fixed or variable noise in contrast discrimination?  
695 The jury's still out.. *Vision Research*, 46(25), 4294–4303.  
696 <http://doi.org/10.1016/j.visres.2005.08.024>
- 697 Graham, N. V. (2011). Beyond multiple pattern analyzers modeled as linear filters (as classical  
698 V1 simple cells): useful additions of the last 25 years. *Vision Research*, 51(13), 1397–  
699 1430. <http://doi.org/10.1016/j.visres.2011.02.007>
- 700 Grill-spector, K., Henson, R., & Martin, A. (2006). Repetition and the brain : neural models of  
701 stimulus-specific effects, 10(1), 17–19. <http://doi.org/10.1016/j.tics.2005.11.006>
- 702 Hecht, S., & Wald, G. (1934). The visual acuity and intensity discrimination of drosophila. *The*  
703 *Journal of General Physiology*, 17(4), 517–547.
- 704 Hesselmann, G., Kell, C. A., Eger, E., & Kleinschmidt, A. (2008). Spontaneous local variations  
705 in ongoing neural activity bias perceptual decisions. *Proceedings of the National*  
706 *Academy of Sciences of the United States of America*, 105(31), 10984–10989.  
707 <http://doi.org/10.1073/pnas.0712043105>
- 708 Hillyard, S. A., Squires, K. C., Bauer, J. W., & Lindsay, P. H. (1971). Evoked potential correlates  
709 of auditory signal detection. *Science (New York, N.Y.)*, 172(3990), 1357–1360.
- 710 Jolij, J., Meurs, M., & Haitel, E. (2011). Why do we see what's not there? *Communicative &*  
711 *Integrative Biology*, 4(6), 764–767.
- 712 King, J., & Dehaene, S. (2014). Characterizing the dynamics of mental representations : the  
713 temporal generalization method, 18(4), 203–210.  
714 <http://doi.org/10.1016/j.tics.2014.01.002> Characterizing
- 715 Kingdom, F. A. A. (2016). Fixed versus variable internal noise in contrast transduction: The  
716 significance of Whittle's data. *Vision Research*, 128, 1–5.  
717 <http://doi.org/10.1016/j.visres.2016.09.004>
- 718 Klein, A., Ghosh, S. S., Bao, F. S., Giard, J., Häme, Y., Stavsky, E., ... Keshavan, A. (2017).  
719 Mindboggling morphometry of human brains. *PLOS Computational Biology*, 13(2),  
720 e1005350. <http://doi.org/10.1371/journal.pcbi.1005350>
- 721 Klein, S. A., & Levi, D. M. (2009). Stochastic model for detection of signals in noise. *Journal of*  
722 *Optical Society of America*, 26(11), 110–126.
- 723 Kleiner, M., Brainard, D. H., & Pelli, D. G. (2007). What's new in Psychtoolbox-3? *Perception*,  
724 36(S), 14.
- 725 Kontsevich, L. L., Chen, C.-C., & Tyler, C. W. (2002). Separating the effects of response  
726 nonlinearity and internal noise psychophysically. *Vision Research*, 42(14), 1771–1784.
- 727 Legge, G. E., & Foley, J. M. (1980). Contrast masking in human vision. *Journal of the Optical*  
728 *Society of America*, 70(12), 1458–1471. <http://doi.org/10.1364/JOSA.70.001458>
- 729 Maris, E., & Oostenveld, R. (2007). Nonparametric statistical testing of EEG- and MEG-data.  
730 *Journal of Neuroscience Methods*, 164(1), 177–190.  
731 <http://doi.org/10.1016/j.jneumeth.2007.03.024>
- 732 Michelson, C. A., Pillow, J. W., & Seidemann, E. (2017). Majority of choice-related variability  
733 in perceptual decisions is present in early sensory cortex. *Preprint*.
- 734 Mostert, P., Kok, P., & de Lange, F. P. (2016). Dissociating sensory from decision processes in



- 735 human perceptual decision making. *Scientific Reports*, 5(1).  
736 <http://doi.org/10.1038/srep18253>
- 737 Mueller, S. T., & Weidemann, C. T. (2008). Decision noise: An explanation for observed  
738 violations of signal detection theory. *Psychonomic Bulletin & Review*, 15(3), 465–494.  
739 <http://doi.org/10.3758/PBR.15.3.465>
- 740 Oostenveld, R., Fries, P., Maris, E., & Schoffelen, J.-M. (2011). FieldTrip: Open Source Software  
741 for Advanced Analysis of MEG, EEG, and Invasive Electrophysiological Data.  
742 *Computational Intelligence and Neuroscience*, 2011, 1–9.  
743 <http://doi.org/10.1155/2011/156869>
- 744 Peirce, J. W. (2007). PsychoPy—Psychophysics software in Python. *Journal of Neuroscience*  
745 *Methods*, 162(1–2), 8–13. <http://doi.org/10.1016/j.jneumeth.2006.11.017>
- 746 Pelli, D. G. (1985). Uncertainty explains many aspects of visual contrast detection and  
747 discrimination. *Journal of the Optical Society of America. A, Optics and Image Science*,  
748 2(9), 1508–1532. <http://doi.org/10.1364/JOSAA.2.001508>
- 749 Pelli, D. G. (1997). The VideoToolbox software for visual psychophysics: Transforming  
750 numbers into movies. *Spatial Vision*, 10(437–442).
- 751 Ress, D., & Heeger, D. J. (2003). Neuronal correlates of perception in early visual cortex.  
752 *Nature Neuroscience*, 6(4), 414–420. <http://doi.org/10.1038/nn1024>
- 753 Roelfsema, P. R., & Spekreijse, H. (2001). The representation of erroneously perceived stimuli  
754 in the primary visual cortex. *Neuron*, 31(5), 853–863. <http://doi.org/10.1016/S0896->  
755 [6273\(01\)00408-1](http://doi.org/10.1016/S0896-6273(01)00408-1)
- 756 Rolls, E. T., & Baylis, G. C. (1986). Size and contrast have only small effects on the responses  
757 to faces of neurons in the cortex of the superior temporal sulcus of the monkey.  
758 *Experimental Brain Research*, 65(1), 38–48.
- 759 Schölvinck, M. L., Friston, K. J., & Rees, G. (2012). The influence of spontaneous activity on  
760 stimulus processing in primary visual cortex. *NeuroImage*, 59, 2700–2708.  
761 <http://doi.org/10.1016/j.neuroimage.2011.10.066>
- 762 Smith, R. A., & Swift, D. J. (1985). Spatial-frequency masking and Birdsall’s theorem. *Journal*  
763 *of the Optical Society of America. A, Optics and Image Science*, 2(9), 1593–1599.
- 764 Squires, N. K., Squires, K. C., & Hillyard, S. A. (1975). Two varieties of long-latency positive  
765 waves evoked by unpredictable auditory stimuli in man. *Electroencephalography and*  
766 *Clinical Neurophysiology*, 38(4), 387–401.
- 767 Tadel, F., Baillet, S., Mosher, J. C., Pantazis, D., & Leahy, R. M. (2011). Brainstorm: A User-  
768 Friendly Application for MEG/EEG Analysis. *Computational Intelligence and*  
769 *Neuroscience*, 2011, 1–13. <http://doi.org/10.1155/2011/879716>
- 770 Tolhurst, D. J., Movshon, J. A., & Dean, A. F. (1983). The statistical reliability of signals in single  
771 neurons in cat and monkey visual cortex. *Vision Research*, 23(8), 775–785.
- 772 Woldorff, M. (1993). Distortion of ERP averages due to overlap from temporally adjacent  
773 ERPs: Analysis and correction. *Psychophysiology*, 30, 98–119.
- 774  
775

776 **6 Appendices**

777

778 Table A1: Numbers of vertices on the cortical mesh. Individual regions were taken from a mesh consisting of  
 779 around 3000 vertices, and pooled across hemispheres. The 'whole brain' mesh (final row) was subsampled to  
 780 around 500 vertices. Precise numbers of vertices varied across individual participants owing to individual  
 781 differences in brain size and morphology. Entries in the 'Colour' column correspond to the colours used in  
 782 Figures 6, A2 & A3.

Region	Colour	Mean size	Minimum size	Maximum size
Rostral Middle Frontal		157	145	173
Superior Frontal		342	317	384
Rostral Anterior Cingulate		31	27	37
Lateral Orbitofrontal		100	83	113
Medial Orbitofrontal		53	45	62
Pars Triangularis		63	56	69
Pars Orbitalis		31	27	35
Caudal Anterior Cingulate		29	25	34
Pars Opercularis		53	43	61
Caudal Middle Frontal		75	59	91
Insula		60	53	69
Entorhinal		16	9	25
Pre-central		140	124	155
Superior Temporal		166	150	183
Posterior Cingulate		38	32	45
Transverse Temporal		9	6	11
Post-central		142	130	156
Para-central		48	41	61
Middle Temporal		134	123	152
Parahippocampal		21	17	25
Inferior Temporal		118	96	149
Supramarginal		123	102	155
Isthmus Cingulate		28	23	34
Fusiform		81	73	87
Precuneous		119	93	140
Superior Parietal		148	136	168
Inferior Parietal		149	131	157
Lingual		101	69	125
Cuneus		67	58	74
Peri-calcarine		38	24	45
Lateral Occipital		162	139	181
Whole brain		503	503	504

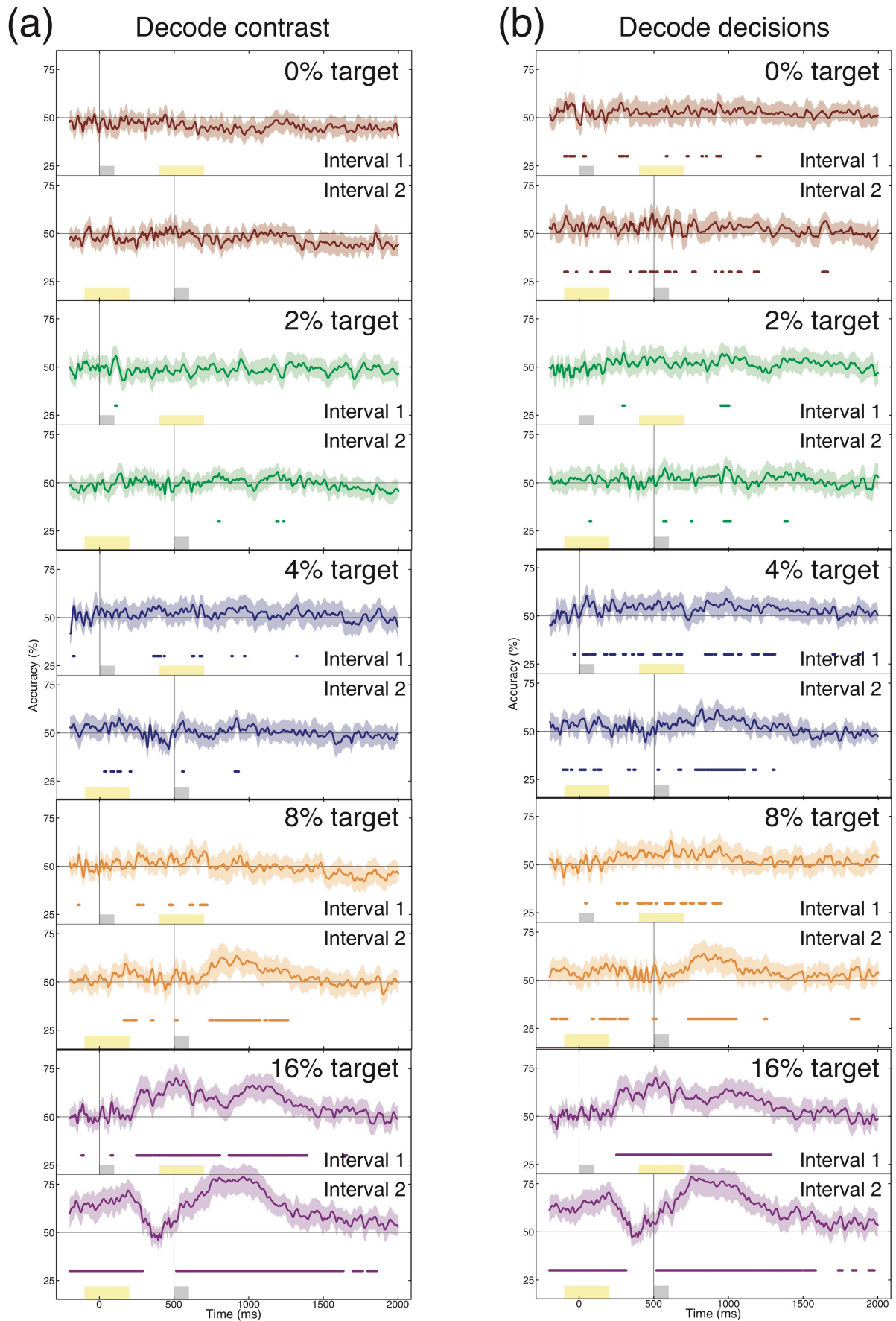
783

784

785

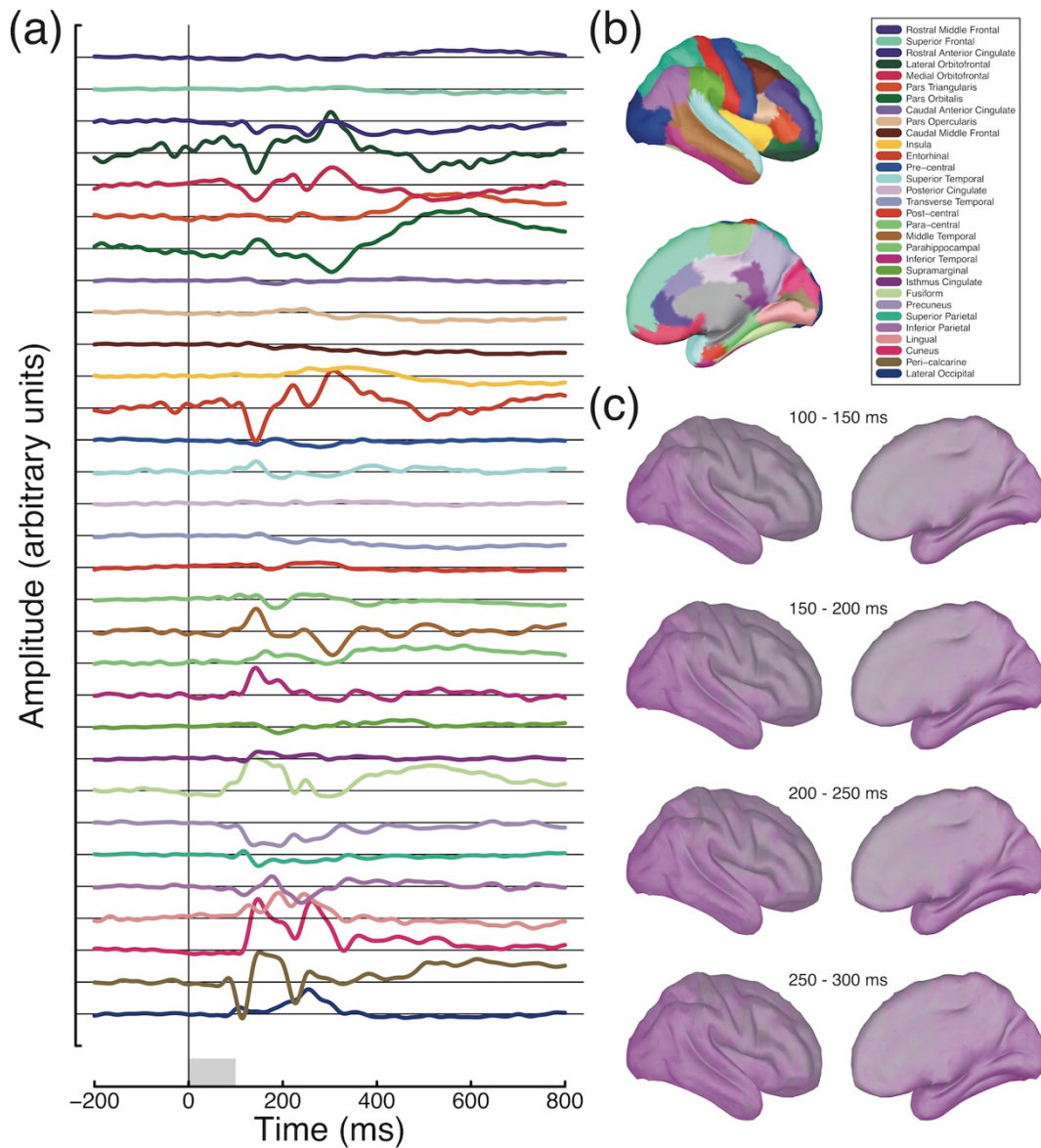
786





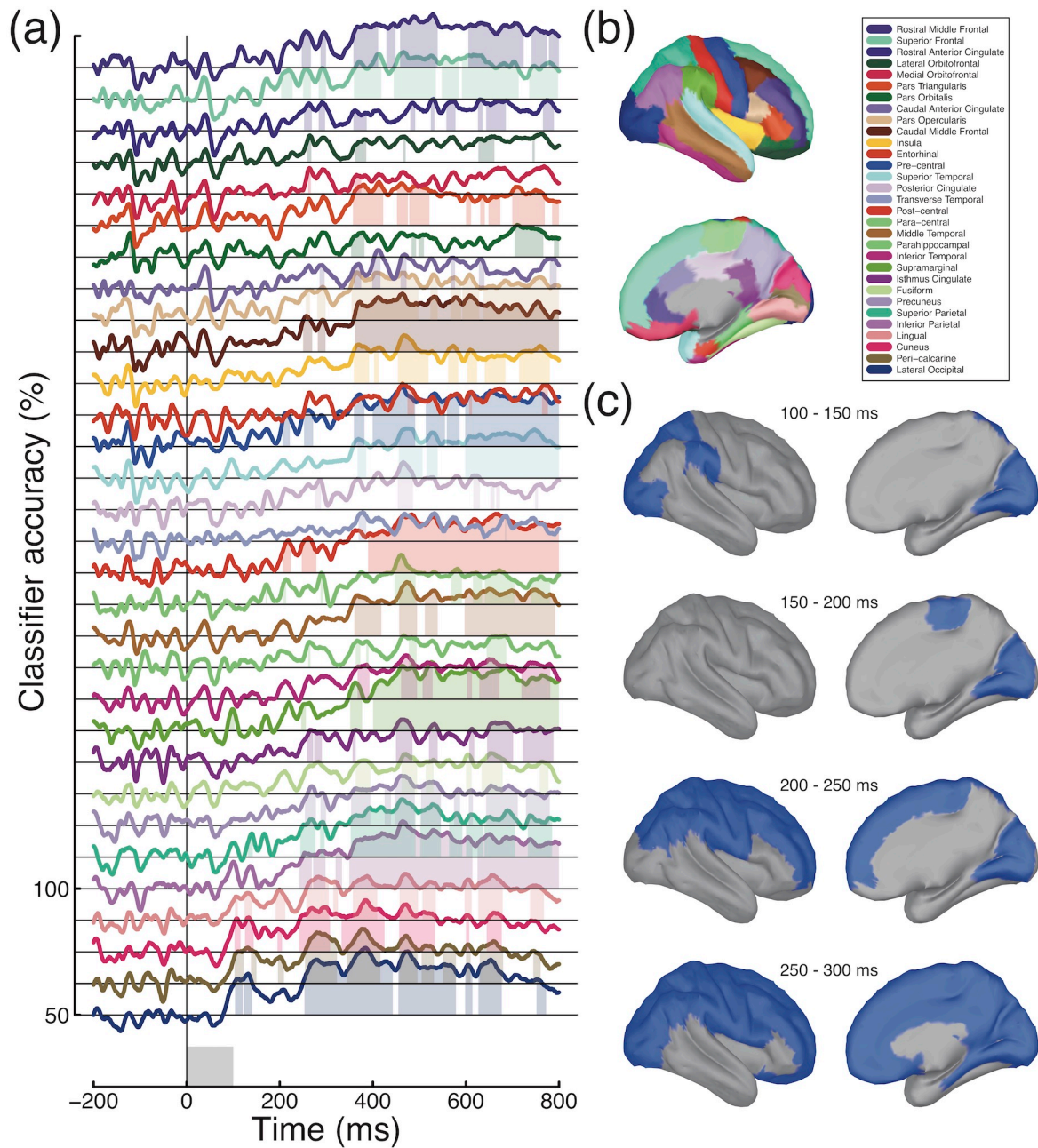
787  
788  
789

Figure A1: Interval-based MVPA analysis for all target contrast conditions, and for both contrast-based decoding (a) and decision-based decoding (b). Plotting conventions are consistent with Figure 4b,c.



790  
791  
792  
793  
794  
795

Figure A2: Maximal evoked responses in different anatomical regions. Each trace in panel (a) plots the timecourse of the vertex in the named region (see legend in panel (b)) with the largest absolute deflection from baseline. Panel (c) shows absolute activity averaged across four time windows, demonstrating that the majority of activity occurs in occipito-temporal regions.



796  
797  
798  
799

Figure A3: Atlas-based classification of decisions in the 16% target condition. Plotting conventions mirror those of Figure 6.